

Quantifying the morphology of flow patterns in landslide-affected and unaffected soils

Christina Bogner^{a,*}, Folkert Bauer^b, Baltasar Trancón y Widemann^c, Pablo Viñan^d, Luis Balcazar^d, Bernd Huwe^b

^a*Ecological Modelling, BayCEER, University of Bayreuth, Dr.-Hans-Frisch-Straße 1–3, 95448 Bayreuth, Germany*

^b*Department of Soil Physics, BayCEER, University of Bayreuth, 95440 Bayreuth, Germany*

^c*Programming Languages and Compiler Technology, Technische Universität Ilmenau, Ehrenbergstr. 29, 98693 Ilmenau, Germany*

^d*Universidad Nacional de Loja, Loja, Ecuador*

Abstract

In mountainous regions, landslides are a common natural phenomenon. They are often triggered by a combination of steep relief and long lasting rainfalls. Therefore, hydrological conditions in the soil are crucial for their initiation. Because direct measurements of water flow are difficult and model predictions uncertain, we used a dye to visualise flow patterns directly. We combined dye tracer experiments with field observations (root density and rock fragment content) and measurements of soil properties (bulk density, soil water retention curve and saturated hydraulic conductivity). We quantified the morphology of flow patterns by image indices and mutual information that measures the overall dependency between variables and compared two shallow landslides of different ages with a landslide-unaffected hillslope. Our results showed that flow patterns on the landslides were more fragmented and contained larger stained objects than on the landslide-unaffected site. We relate these findings to a larger stone content and a stronger macropore–soil matrix interaction. Moreover, we detected a fissure network on the younger landslide that probably affects its hydrological behaviour. Field observations, soil hydraulic properties and dye tracer studies describe different hydrological aspects of the studied sites and complement the information provided by the morphological image indices.

Keywords: flow patterns, tropical montane forest, shallow landslide, dye tracer, morphological image indices, mutual information

1. Introduction

Landslides are a ubiquitous phenomenon in mountainous regions. They may cause severe damage and have been studied as part of the Unesco's earth science programme for several decades (e.g. [Varnes, D.J. and the International Association Of Engineering Geology](#)

*Corresponding author: Tel.: +49 921 555655; Fax: +49 921 555799

Email address: christina.bogner@uni-bayreuth.de (Christina Bogner)

Commission on Landslides and Other Mass Movements on Slopes, 1984). The term landslide stands for any mass movement of rock, debris or earth down a slope (Cruden, 1991) that is caused by slope instability. This instability might arise from human activities like road construction or deforestation, or natural processes like increasing weight due to vegetation growth or precipitation (Crozier, 1986). As a major (natural) disturbance, landslides appear to play an important role in maintaining a high plant species diversity in tropical montane forests (e.g. Garwood et al., 1979; Guariguata, 1990; Kessler, 1999). More general, in some areas landslides deeply affect the evolution of the landscape (Cendrero and Dramis, 1996).

In the Andes of South Ecuador landslides are a common phenomenon frequently occurring in undisturbed mature forests. These landslides are mainly initiated by the combination of steep relief and long-lasting rainfalls (Wilcke et al., 2003). Additionally, Bussmann et al. (2008) reported that sliding activity was particularly intensified by earthquakes frequently occurring in this area. The heterogeneous mixture of substrates caused by landslides contributes to small-scale variation of soil properties (Lundgren, 1978; Adams and Sidle, 1987).

For rainfall-induced landslides, hydrological conditions in the soil like soil moisture distribution are crucial (Guzzetti et al., 2008, and references therein). Water flow in soils as well as the distribution of flow paths influence the soil moisture. We can distinguish two rather different flow types: water can percolate slowly through the soil matrix (matrix flow) or move rapidly through preferred pathways and bypass a large portion of the soil (preferential flow). Soil structure promote preferential flow, and roots and stones often serve as the main flow paths (e.g. Jarvis, 2007; Sauer and Logsdon, 2002).

In general, direct measurements of water flow are difficult and model predictions uncertain. This is especially true for heterogeneous landslide-affected soils. Therefore, dyes are often used in tracer experiments to visualise flow patterns directly (e.g. Flury et al., 1994; Noguchi et al., 1999). The main outcome of such studies are high-resolution digital photographs of dye-stained patterns. To our knowledge, no agreed objective criteria to analyse and compare such images exist in the soil hydrology community. Therefore, in a recent paper, Trancón y Widemann and Bogner (2012) proposed several morphological image indices to extract hydrologically relevant information from such images.

In the present work, we use image indices for both, a quantitative analysis of flow patterns and a comparison between study sites via principal component analysis. We combine dye tracer experiments with field observations from stained soil profiles (root density and rock fragment content) and measurements of soil properties (bulk density, soil water retention curve and saturated hydraulic conductivity). Our goal is to quantify the morphology of flow patterns (i.e. the amount of staining and its structure) in shallow landslides of different ages and to compare it with that on a landslide-unaffected gentle hillslope.

2. Material and methods

2.1. Study area

The study area is located in the Reserva Biológica de San Francisco (RBSF, 3°58'30" S and 79°4'25" W) surrounding the research station Estación Científica San Francisco (ECSF) (Figure 1). This area of 11.2 km² is part of the eastern slope of the Cordillera Real and is situated at about 2000 m above sea level (ASL). It is characterised by steep slopes (30–50°) and a natural vegetation cover of evergreen montane forests (Balslev and Øllgaard, 2002).

The RBSF has been studied intensively for several years and an extensive collection of results can be found in [Beck et al. \(2008\)](#) and [Bendix et al. \(2013\)](#).

In the study area, only the north-facing slope of the east–west striking Rio San Francisco valley is forested by mostly undisturbed natural forest. The most important tree families are Lauraceae, Rubiaceae, Melastomataceae and Euphorbiaceae often bearing vascular epiphytes ([Paulsch, 2002](#)). The ground vegetation layer is dominated by ferns and large herbs ([Homeier et al., 2002](#); [Paulsch, 2002](#)), particularly Dryopteridaceae and Lobeliaceae. In contrast, the foot slopes of the north-facing valley side and the south-facing part have been cleared by slash and burn and are now covered by fallows and pastures of different ages ([Werner et al., 2005](#)).

Between 1998 and 2005 the mean annual precipitation equalled about 2200 mm, with the main rainy season occurring from April to July ([Rollenbeck et al., 2007](#)). From 1998 to 2000 the mean annual air temperature equalled 16.2 °C ([Fleischbein et al., 2005](#)).

The bedrock of the RBSF belongs to the Chiguinda unit (within the Zamora series) consisting of interbedded paleozoic phyllites, metasandstones and quartzites ([Hungerbühler, 1997](#)). The natural vegetation cover has been removed in several areas by landslides occurring frequently in this region. Most of these mass movements are translational slides ([Cruden and Varnes, 1996](#)), intermediate between translational debris slides and rapid earth flows ([Wilcke et al., 2003](#); [Busmann et al., 2008](#)). They are typically shallow and can be roughly divided into an upper depletion and a lower accumulation zone ([Cruden and Varnes, 1996](#)). In 1998, for example, visible landslides covered 3.7% of the RBSF ([Wilcke et al., 2003](#)). Their deposits consist of a mixture of fine soil material and a varying amount of phyllites, metasiltsstones and sandstones of different sizes and shapes ([Wilcke et al., 2003](#)).

The soils within the RBSF are generally shallow and loamy-skeletal ([Yasin, 2001](#)) and have developed mostly from landslide deposits and probably periglacial sediments ([Wilcke et al., 2001](#)). Aside the landslide-affected hillslopes, Stagnosols and Histosols with stagnic colour pattern frequently occur above 2100 m ASL under natural forest ([Liess et al., 2009](#)).

2.2. *Experimental sites*

We worked on eight different experimental plots situated in the southern part of the ECSF between 1900 and 2100 m ASL (Figure 1). We picked out two landslides with slopes ranging between 20° and 40° as they typically occur in this area.

Two experimental plots were chosen on a young landslide (YL) formed in 1998 (Figure SF3 in the online Supplementary Material): the first one within the depletion (YL_DEPL) and the second one in the accumulation zone (YL_ACC). Additionally, four plots were selected on an old landslide (OL): two in the depletion zone (OL_DEPL A and OL_DEPL B) and two in the accumulation zone (OL_ACC A and OL_ACC B). The plots A and B were situated approximately 20 m apart from each other. Aerial photographs revealed that the old landslide must have been formed before 1962. Additionally, soil profile surveys indicated at least two slide events. The landslides presented in this paper were not triggered by human activities like road building, for example.

The last two experimental plots (PA 1 and PA 2) were established between 2050 and 2200 m ASL in a mature ridge forest. Here, the slopes ranged between 5° and 15°. We consider this area as landslide-unaaffected and call it in the following plateau area (PA).

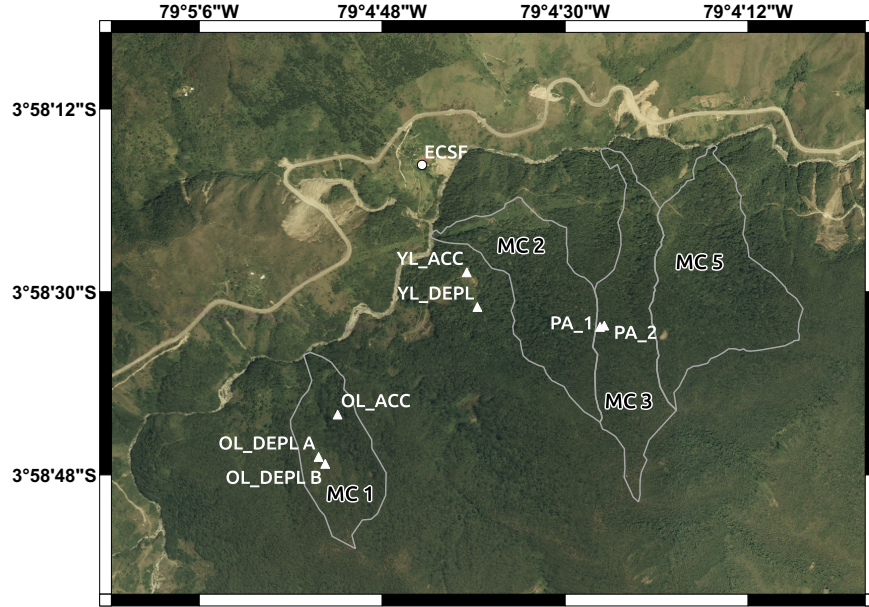


Figure 1: Map of the ECSF investigation area (geographic coordinates EPSG:4326). The triangles indicate the position of the experimental plots. Boundaries of microcatchments (MC 1, MC 2, MC 3 and MC 5) show landscape units studied in [Beck et al. \(2008\)](#) and [Bendix et al. \(2013\)](#).

We are aware that the comparison of flow patterns on hillslopes of different inclinations is difficult. However, we have chosen these sites because they are representative for the study area.

2.3. Tracer infiltration experiments

At each plot we carried out dye tracer experiments (between September and December 2006), took undisturbed and disturbed soil samples and characterised several soil profiles and the vegetation in the vicinity. We applied 200 litres of a Brilliant Blue FCF solution with a concentration of 10 g l^{-1} in 1.5 h using a static line source sprinkler. It consisted of a water conducting tube with diameter and length of 2.5 cm and 1.5 m, respectively. Without moving the tube, the dye tracer solution was irrigated homogeneously on a surface of approximately $20 \times 170 \text{ cm}$ by six fan nozzles installed equidistantly from each other along the tube. A similar sprinkler was used by [Noguchi et al. \(1999\)](#) to investigate lateral flow paths in a forested hillslope. During the irrigation we kept the pumping rate constant. We used Brilliant Blue FCF as dye tracer because it has acceptably low toxicity and a good visibility against the background colour of most soils (e.g. [Flury et al., 1994](#)).

Immediately after the irrigation, we covered each plot by a $3 \times 3 \text{ m}$ plastic tarp to prevent infiltration of subsequent rainfall. On the following day we opened a pit and prepared the first soil profile 200 cm downwards and parallel to the sprinkler. The subsequent profiles followed in steps of 20 cm towards the sprinkler. Sometimes we had to excavate in steps of up to 40 cm or were unable to excavate because of big rock fragments or a thin mineral soil. After preparing a profile, we placed a 1 m^2 metallic frame in front of it and took a photograph using a Canon Coolpix 4500 digital camera with a resolution of 1200×1600 pixels. The frame delimited the region of interest that we wanted to analyse.

On OL_ACC A and OL_ACC B the soil profiles were highly unstable and we could only prepare three and four profiles, respectively. Therefore, for further analysis we merged the images (where possible) and call this data set OL_ACC.

In the immediate vicinity of each plot, we measured the (field) saturated hydraulic conductivity (K_s) in situ with a compact constant head permeameter (Amoozometer) (Amoozegar, 1989a). On every study site, we took 23 to 53 measurements in three different depths. To compute the final values of K_s , we used Glover’s equation (Amoozegar, 1989b).

2.4. Soil sampling and laboratory analysis

From the soil profile approximately 1 m downslope from the sprinkler we took undisturbed soil samples (100 cm^3), where possible per horizon otherwise per depth range, to determine the soil water retention curve (SWRC). Additionally, we took disturbed samples for the estimation of the water content at pF 4.2 and texture analysis at the same location as the undisturbed cores. Except on PA 1 and PA 2, the rock fragment content was large and sampling not everywhere possible. On OL_DEPL A and OL_DEPL B, we were unable to take any undisturbed soil cores. Instead, we used the SWRC and texture determined by Markwardt (2005) from a closely situated soil profile.

The water content of the undisturbed samples were evaluated at pF values of 0, 0.5, 1, 1.5 and 2 applying the hanging water column method. For each horizon or depth range, the van Genuchten equation (van Genuchten, 1980) was fitted to the data using the approach implemented in RETC ver. 6 (U.S. Salinity Laboratory, USDA, ARS, Riverside, California, USA), a software to estimate the SWRC and hydraulic conductivity of unsaturated soils.

Bulk densities were determined from the undisturbed samples after 48 h of drying at $105\text{ }^\circ\text{C}$. The texture was analysed by wet sieving of the sand fraction and by the sedimentation method after Köhn (1928) for the silt and clay fractions.

The first, the middle and the last soil profiles of each pit were characterised after the German soil mapping guidelines (AG Boden, 2005) corresponding in general to the guidelines of soil description of the FAO (FAO, 2006). The rock fragment content and the root density were estimated in the field. The soil colour was determined on wet samples after Munsell soil colour chart (Oyama and Takehara, 1999). Soil type and horizons were named according to IUSS Working Group WRB (2007). Since no obvious differences between profiles within the same pit were observed, we merged the data for the sake of clarity.

3. Image analysis

3.1. Image classification

We corrected the lens distortion of the photographs using the software PTLense (Niemann, T., ePaperPress.com, Portland, Oregon, USA). Subsequently, we corrected the images for geometric distortion and classified them in Brilliant Blue stained and non-stained areas in HALCON (MVTec Software GmbH, Munich, Germany). First, we transformed the images from RGB to HSI (Hue, Saturation, Intensity) colour space because the latter is more suitable for a robust separation of colours under varying illumination (MVTec Software GmbH, 2007). Subsequently, we classified all pixels in a certain colour range as stained and thus converted the photographs into binary images. Finally, we corrected misclassification due to shadows or rock fragments manually.

The soil surface at the experimental sites was uneven. This means that the top of the binary images contained pixels that were not part of the soil profile. Therefore, we had to crop the images to exclude these areas. However, except for one image on YL_DEPL (it showed a deep depression) this cropping was minor compared to the image size.

3.2. Quantification of pattern morphology via image indices

To discern hydrologically relevant information from binary images some kind of feature (i.e. property) extraction is necessary. [Tracón y Widemann and Bogner \(2012\)](#) introduced image index functions (or indices) to analyse images of dye tracer infiltration studies. In a related publication, [Bogner et al. \(2013\)](#) showed how these indices could be used for classification of flow patterns. Image indices are real-valued functions in the range $[0, 1]$ that calculate certain properties of binary images and thus provide quantitative information about the morphology of flow patterns. Here, we describe them briefly. A detailed introduction and an example calculation of image indices are given in the online Supplementary Material (Section 1.2).

The *dye coverage* I_D is the classical index used to summarise the information of a binary image of a stained soil profile. It shows the proportion of staining, but cannot distinguish between different pattern configurations (e.g. whether a pattern is contiguous or fragmented).

We call (maximal) contiguous subvectors of equal values “runs”. The length of runs of 1s shows the widths of stained objects. To summarise the distribution of runs in a robust manner we calculate their 5%, 50% (i.e. median) and 95% quantiles that we name the (robust) *minimum* $I_{Q0.05}$, *median* $I_{Q0.5}$ and (robust) *maximum width of stained objects* $I_{Q0.95}$. The number of runs is called I_E .

I_F measures the fragmentation of the stained patterns. Given two rows with the same amount of staining (i.e. equal I_D), I_F will be smaller for patterns with larger maximum run length $I_{Q0.95}$.

Finally, the metric entropy I_{MEL} allows to assess the correlation structure inside words of length L (i.e. subvectors of image rows). It is based on Shannon’s entropy that describes the average information content of a random variable. Metric entropy attains its maximum when single pixels in the words are uncorrelated and decreases for correlated pixels. For larger L we need more data to avoid finite size effects. In our study, the length of the image rows equals approximately 1400. Therefore, following [Wolf \(1999\)](#), we chose $L = 12$.

3.3. Principal component analysis

Every experimental site yielded a number of binary images and thus a collection of image indices. To assess possible differences between sites, we examined the results of a principal component analysis (PCA) of these collections (e.g. [Borg and Groenen, 2005](#)). The distribution of the indices can influence the results of the PCA. [Pyle \(1999\)](#), for instance, emphasised that some techniques had equal sensitivity to all values across the whole range. Actually, for the PCA all values are equally important because it uses Euclidean distances to infer their proximity. However, some values of the indices are more frequent and tend to dominate the distribution (e.g. zeros for completely non-stained image rows) thus possibly masking interesting structures. Therefore, we transformed the values to approximate a uniform distribution in the range $[0, 1]$. Figure 4 and Supplementary Figure SF4 show the violin plots of the original and the transformed indices. A violin plot is a combination of a box-plot and a rotated density plot ([Hintze and Nelson, 1998](#)).

The transformed image indices were organised in a matrix of size $\sum_i l_i \times 7$, where l_i is the height of image i , 7 is the number of image indices used, and the PCA was calculated for every site separately on the correlation matrix (except for OL_ACC A and OL_ACC B that were merged). The importance of each principal component (PC) can be assessed via the explained variance:

$$\text{var} = \frac{\lambda_i}{\sum_i \lambda_i}, \quad (1)$$

where λ_i is the i th eigenvalue corresponding to the i th PC.

To provide confidence intervals for the estimates of eigenvalues and eigenvectors we used bootstrap resampling (Efron and Tibshirani, 1986; Jackson, 1993). 5000 matrices of the same size as the original matrix were sampled with replacement from the transformed image indices and the PCA was recalculated. Because the sign of the eigenvectors is arbitrary, every new computation of the PCA can lead to axis reversal or reflection and alter the calculation of confidence intervals. Therefore, bootstrapped eigenvectors were aligned with the original eigenvectors by multiplying them with -1 where necessary (Mehlman et al., 1995). Finally, the confidence intervals were evaluated as the 5% and 95% quantiles. Following Jackson (1993), eigenvector coefficients with confidence intervals not overlapping zero can be interpreted.

3.4. Mutual information between morphological image indices

Since our tracer experiments took place on slopes, the flow patterns might change in an interesting way with the distance to the sprinkler. We describe the patterns by image indices and to assess their change we need some measure of correlation between these indices. However, different correlation coefficients measure different kind of correlations (e.g. Pearson's correlation coefficient is only sensitive to linear correlation). Because we do not know which kind of relationship exists between indices, we chose a measure that is quite general, namely mutual information. For two random variables, it equals

$$I(X, Y) = H(X) + H(Y) - H(X, Y) \quad (2)$$

where $H(X)$ and $H(Y)$ are the Shannon entropies of X and Y , respectively (c.f. equation (SE7) in the online Supplementary Material), and $H(X, Y)$ is the joint Shannon entropy of X and Y .

We estimated the mutual information by the method of k -nearest neighbours (Kraskov et al., 2004). It avoids the binning (discretization) of the real-valued indices that is known to produce biased estimates (Kraskov et al., 2004). The calculations were done using the R-package `parmigene` (Sales and Romualdi, 2012).

The mutual information is non-negative, but has no upper bound, which complicates comparisons between different indices or experimental sites. Therefore, we normalised the mutual information (Joe, 1989):

$$I^*(X, Y) = \text{sign}(\hat{I}(X, Y)) \left(1 - e^{-2|\hat{I}(X, Y)|}\right)^{\frac{1}{2}}, \quad (3)$$

where $\hat{I}(X, Y)$ is the estimate of the mutual information and the function $\text{sign}(\cdot)$ evaluates the sign of its argument. In contrast to Joe's original definition, we take into account possible

estimation inaccuracies of $I(X, Y)$ by using the function $\text{sign}(\cdot)$ (Numata et al., 2008). Indeed, although $I(X, Y) \geq 0$, the estimate $\hat{I}(X, Y)$ might be negative indicating estimation errors. A normalisation with the sign function allows for negative values if $\hat{I}(X, Y) < 0$. If $\hat{I}(X, Y) \geq 0$, then $I^*(X, Y) \in [0, 1]$. $I^*(X, Y)$ measures the overall dependency between X and Y and shows how well Y can be predicted knowing X . It is 0 if and only if X contains no information about Y (i.e. X and Y are statistically independent), will approach 1 for increasing $\hat{I}(X, Y)$ and equals 1 if there is a perfect functional relationship between X and Y . If X and Y are normally distributed, $I^*(X, Y)$ becomes the absolute value of the linear (i.e. Pearson) correlation coefficient (Joe, 1989).

As explained in 3.1 some images were cropped to correct for uneven soil surface. Additionally, when taking pictures in the field it is difficult to position the frame exactly at the same level in front of all profiles. To assess how this involuntary “shifting” of images affects the mutual information we compared $I^*(X, Y)$ calculated on whole images with $I^*(X, Y)$ calculated on images shifted by different amounts against each other.

4. Results

4.1. General site description, soil physical and hydraulic properties

Young landslide. The vegetation cover on YL_ACC consisted of herbage, fern and bushes accompanied by patches of vegetation-free organic layer (≤ 10 cm thick). On YL_DEPL, the vegetation thinned out leaving space for a patchy light grass cover and bare soil encrusted by lichens and mosses. An organic layer was absent. Small rock fragments at the soil surface formed a network of rills and gullies, some charged with gravel. In some places, we found shallow deposits of bare silt and fine sand.

The soil texture on YL was classified as silt loam based on the USDA soil texture classes (Table 1). Animal burrows as well as notable soil fauna (e.g. earth worms, ants or termites) were mostly absent. The volumetric content of rock fragments exceeded 30% and increased with depth (Table 2). These rock fragments consisted of a mixture of angular, weakly metamorphic siltstones and phyllites and belonged mainly to the gravel class (2–64 mm in diameter). However, we also found single rock fragments of up to 40 cm in diameter. In contrast, the root counts decreased with depth.

We found a sharp boundary between the mineral soil and the weathered parent material on YL_DEPL in 25–60 cm depth. This might be due to the sliding process during which the mineral soil was abraded till the more resistant, less weathered and impervious parent material. In contrast, on YL_ACC the transition to the parent material was absent within the excavated depth.

The gentle slope of the SWRC on YL indicated that the soil contained many smaller pores (Figure 2). Indeed, it retained much of its water at large pF values and attained a residual water content of about 0.2. Especially in the soil below 20 cm depth, the SWRC is extremely flat. The hydraulic capacity curve (i.e. $d\theta/dh$, the slope of the soil water retention curve) shows the rate of change in water content with changing matric pressure h . The largest changes occurred between pF 1 and pF 2. This range of matric pressure corresponds to an equivalent pore radius of approximately 0.1 to 0.01 mm (e.g. Nimmo, 1997). The median values of K_s were comparable between YL_DEPL and YL_ACC (6–8 mm h⁻¹ and 4–6 mm h⁻¹, respectively) and remained constant with depth.

Old landslide. On OL_ACC a secondary forest (between 20 and 25 years old) with closed canopy dominated and the mineral soil was entirely covered by at least a 10 cm thick organic layer. To the contrast, on OL_DEPL bushes, grasses and particularly fern abounded with only few single young trees. An organic layer was throughout present ranging in thickness between a few cm under grass and up to 50 cm under fern.

On OL_DEPL B, a part of the dye tracer flowed laterally between the organic layer and the mineral topsoil. This implies a lower infiltrability of the mineral topsoil compared to OL_ACC, where such a subsurface flow was not observed. Indeed, although the soil surface on OL_DEPL B appeared even, the surface of the mineral soil underneath the organic layer was rough and contained a large depression. The subsurface flow of the dye tracer occurred mainly there. The upper part of the topsoil in the depression contained less rock fragments and could be clearly distinguished from the soil underneath, where a buried A horizon (Ahb) was found (Table 2, OL_DEPL B). Therefore, we concluded that this material originated from a small (local) landslide event.

In contrast to YL_DEPL, we observed a smooth transition between the mineral soil and the weathered bedrock on OL. On OL_ACC, for example, a 20 cm large transition zone developed in 80 cm depth, where the weathered parent material set in gradually. A part of the dye tracer flowed there laterally downhill.

The provenance of the material on OL_DEPL B below 70 cm depth remained ambiguous. It contained less than 10% in volume of fine soil and showed neither a bedding structure nor a clear alignment of the rock fragments, which ranged between 10 and 40 cm. This material could be a strongly weathered parent material or landslide deposits.

Similar to YL, the soil texture on OL was classified as silt loam. However, the clay content was larger (8–13% on YL and 12–21% on OL, respectively). The rock fragment content exceeded 30% and increased with depth. Particularly on OL_DEPL, we found more larger rock fragments. The root counts were comparable to those on YL_ACC and decreased with depth in a similar way.

The median values of K_s were several orders of magnitude larger than on YL. In general, the conductivity decreased with depth and varied most in about 25 cm depth. On OL_DEPL the form of the SWRC showed the presence of larger pores (equivalent pore radius > 0.1 mm). In contrast, the SWRC and hydraulic capacity in the accumulation zone were similar to the ones on YL_DEPL above 20 cm depth.

Plateau area. The forest canopy on PA was open while the shrub layer consisting mainly of Bromeliaceae and Orchidaceae was dense. The thickness of the organic layer equalled 33 cm on the average, but could range up to 45 cm. Similarly to OL_DEPL B, a part of the tracer flowed laterally between the organic layer and the mineral topsoil.

We found the lowest root counts and the smallest rock fragment content on PA. The sand fraction dominated in the topsoil classified as sandy loam (Tables 1 and 2). The steeper slope of the SWRC in the topsoil accords well with this larger sand content. Deeper in the soil the clay fraction increased and the textural class changed to loam, which agrees with a flatter SWRC. The median values of K_s were small, however, some measurements in 20 cm and 40 cm

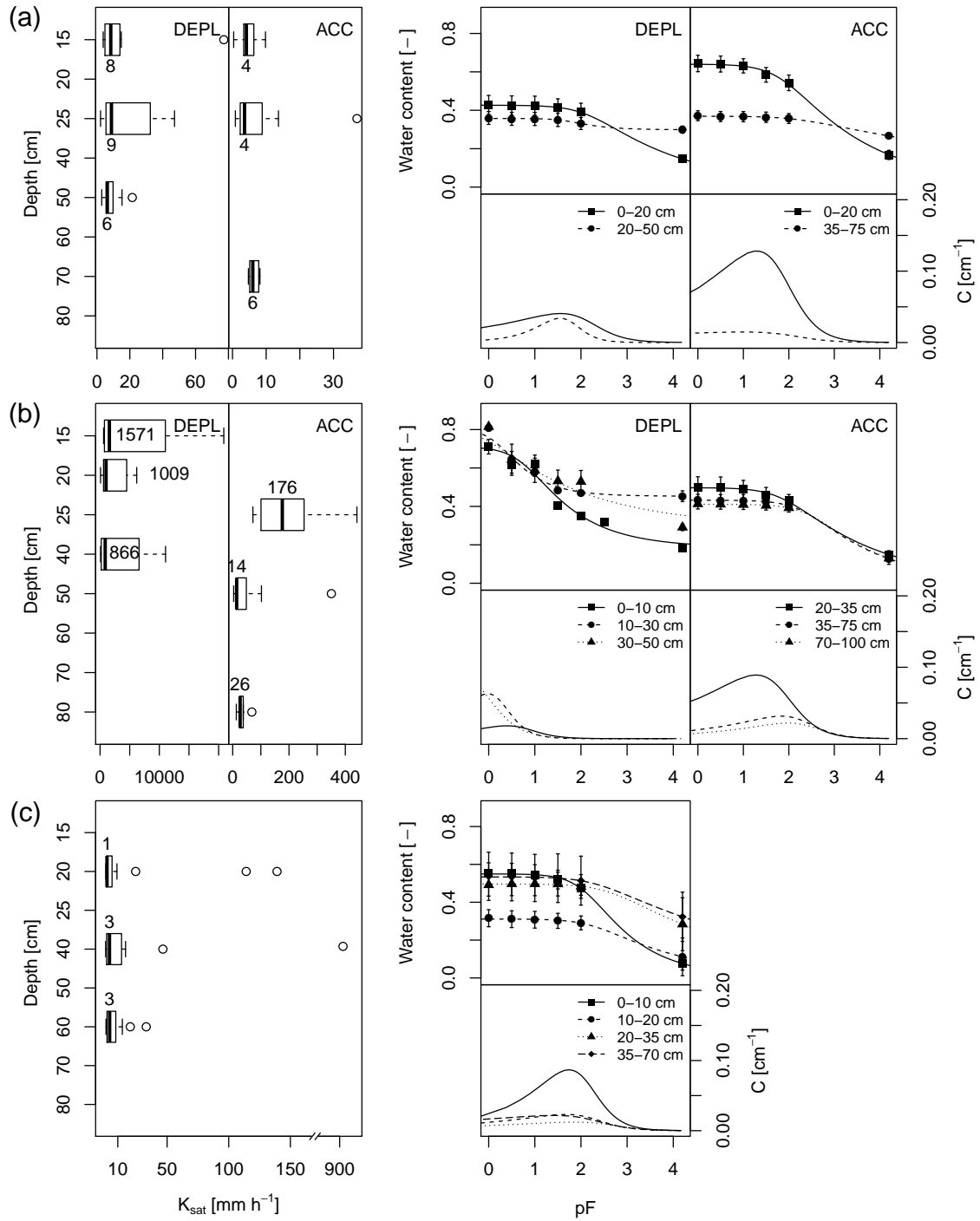


Figure 2: Saturated conductivity K_s (left), soil water retention and hydraulic capacity C (right) on YL (a), OL (b) and PA (c). Note that $C = d\theta/dh$ is the derivative of the water content with respect to matric pressure h and not with respect to pF value. DEPL and ACC denote the depletion and accumulation zones, respectively, PA 1 and PA 2 were merged. Values next to boxes in the left column are medians of K_s . The curves in the right column were modelled, the symbols show measured data and the error bars their standard deviations. The measurements of soil water retention on OL_DEPL were taken from [Markwardt \(2005\)](#).

Table 1: Particle size distribution (mean values \pm standard deviations). Rows not summing to 100 indicate inaccuracies in the measurements.

Site	Depth range (cm)	Sand (%)	Silt (%)	Clay (%)
YL_DEPL	0–10	38 \pm 4	54 \pm 4	9 \pm 3
	20–30	30 \pm 11	59 \pm 8	11 \pm 6
	30–50	36 \pm 4	55 \pm 4	9 \pm 1
YL_ACC	0–10	34 \pm 7	55 \pm 4	11 \pm 3
	10–20	36 \pm 6	54 \pm 4	11 \pm 2
	30–50	33 \pm 4	54 \pm 4	13 \pm 7
	50–60	33 \pm 2	59 \pm 2	8 \pm 1
OL_DEPL ^a	0–10	31 \pm 2	53 \pm 3	16 \pm 3
	10–30	35 \pm 9	50 \pm 4	15 \pm 6
	30–50	28 \pm 3	59 \pm 5	13 \pm 3
	50–65	28 \pm 11	61 \pm 10	12 \pm 2
OL_ACC	20–40	26 \pm 3	56 \pm 8	18 \pm 7
	50–70	27 \pm 2	52 \pm 2	21 \pm 1
	70–90	28 \pm 1	53 \pm 3	20 \pm 3
	90–100	26 \pm 2	54 \pm 4	19 \pm 3
PA	0–10	56 \pm 3	35 \pm 4	9 \pm 1
	10–20	56 \pm 3	36 \pm 3	8 \pm 2
	20–40	37 \pm 13	39 \pm 14	24 \pm 11
	40–70	32 \pm 22	51 \pm 14	17 \pm 10

^a determined by [Markwardt \(2005\)](#)

depth exceeded the median by several orders of magnitude.

4.2. Morphology of flow patterns

4.2.1. In the soil profile

Young landslide. On YL_DEPL Brilliant Blue infiltrated till the weathered bedrock situated in 25–60 cm depth (Figure 3 and Supplementary Figure SF5). In the proximity of the sprinkler we were unable to prepare soil profiles because the mineral soil was too thin and we could not dig into the bedrock. Therefore, only images between 200 cm and 120 cm are available.

The flow patterns appeared fragmented ($Q_{0.5}(I_F) = 0.86$) throughout the profile with a relatively constant metric entropy I_{ME12} . The number of stained objects I_E remained small and their maximal width $I_{Q0.95}$ did not exceed 0.35 (i.e. 35% of the image width). Because the minimum $I_{Q0.05}$ and the median run lengths $I_{Q0.5}$ were similar and small we conclude that at least half of the stained objects were small (cf. Figure 4 and Supplementary Table ST3 for empirical distributions of indices).

On YL_ACC we could detect the dye down to the bottom of the profiles in approximately 1 m depth (Figure 3 and Supplementary Figure SF6). In general, I_D decreased with depth and was smaller than on YL_DEPL ($Q_{0.5}(I_D) = 0.20$). This decrease with depth coincides with a declining root density (Table 2) and could indicate that the flow converged to preferential flow paths along root macropores after infiltration. Moreover, we found a network of fissures some of them reaching from the ground surface down to more than 100 cm (Supplementary Figures SF13 and SF14) that were intensely stained.

In some profiles between 20 cm and 50 cm depth we found remnants of a buried A horizon mixed with an organic layer. These areas were almost completely stained causing $I_{Q0.95}$ to increase. Compared to YL_DEPL, there were also fewer stained objects (smaller I_E) (Figure 4), and I_F and I_{ME12} varied stronger throughout the profiles. Except in one profile

Table 2: Data from soil profile descriptions and laboratory analysis. Soil type and horizons were named according to [IUSS Working Group WRB \(2007\)](#). Depth shows the lower horizon boundary and the last column indicates the number of bulk density samples.

Horizon	Depth (cm)	Soil colour	Volumetric rock fragment content (%)	Counts of roots (dm ⁻²)	Bulk density ± stand. dev. (g cm ⁻³)	n
YL-DEPL; Haplic Regosol (skeletic, siltic); slope approx. 35°; aspect N, OL absent						
C	0-25 25-60	10 YR 5/4	50	3-5 ^a 1-2 ^a	1.46±0.14	5
2C	>60	2.5 Y 6/3	residual rock structure	0	1.73±0.09	5
YL-ACC; Haplic Regosol (skeletic, siltic); slope approx. 25°; aspect NE, OL approx. 10 cm thick						
A ^a	1-10	10 YR 4/4	30	6-10	0.85±0.12	5
Ob+Ahb ^a	20-50	7.5 YR 3/3	-	50+6-10	0.68±0.25	4
C	>80	2.5 Y 6/3	50	3-5 ^b 1-2 ^{a,c}	1.59±0.07	5
OL-DEPLA; Regosol (skeletic, siltic), slope approx 30°; aspect NE, OL approx. 10 cm thick						
C	5-20	10 YR 3/3	50	6-10	0.92±0.11	3 ^d
2C	>80	2.5 Y 6/4	residual rock structure	1-2 ^b	1.27±0.02	2 ^d
OL-DEPLB; Cambisol (skeletic, siltic, novic); slope aprox. 30°; aspect N, OL approx. 10 cm thick						
Ah	10-25	10 YR 3/3	30	6-10	0.93±0.09	5 ^d
Ahb	20-50	10 YR 2/2	75	6-10	-	-
Bwb	35-65	10 YR 4/3	75	3-5	1.28±0.07	2 ^d
Bwb-C	65-75	10 YR 4/6	80	3-5	1.19±0.19	3 ^d
C	>80	-	residual rock structure	1-2 ^{e,a}	-	-
OL-ACC; Cambisol (skeletic, siltic); slope approx. 35°; aspect NW, OL approx. 10 cm thick						
Ah	40-50	10YR 4/3	50	6-10	1.20±0.16	11
Bw	75-90	2.5 Y 5/4	65	3-5	1.45±0.15	9
C	>120	10 YR 5/4	80	1-2 ^f	1.54±0.10	15
PA 1; Histic Stagnosol (albic, endosiltic); slope approx. 5°; aspect N, OL approx. 33 cm thick						
E	0-10 10-20	7.5 YR 3/1 7.5 YR 5/1	<5	3-5 1-2	0.96±0.10 1.74±0.10	5 5
Bg	20-35 35-60	7.5 YR 7/1 5 YR 6/8	<5	0	1.22±0.07 1.03±0.04	5 7
C	>80	-	residual rock structure	0	-	-
PA 2; Histic Stagnosol (albic, endosiltic); slope approx. 5°; aspect NNE, OL approx. 33 cm thick						
E	0-10 10-25	10 YR 3/1 7.5 YR 4/1	<5	3-5 1-2	1.25±0.17 1.71±0.04	5 4
Bg	25-40	10 YR 8/8	<5	0	1.64±0.15	5
C	>80	-	residual rock structure	0	-	5

^a patchy occurrence ^b ≤ 30 cm depth ^c ≤ 50 cm depth ^d some samples contained small rock fragments ^e ≤ 80 cm depth
^f ≤ 90 cm depth

with very large stained objects along a vertical fissure (Supplementary Figures SF6(i) and SF13, $\max(I_{Q0.95}) = 0.5$) and on the top of some profiles, $I_{Q0.95}$ was comparable to YL_DEPL.

Old landslide. On OL_DEPL A only images within 20 cm to 100 cm from the sprinkler were available because of large stones. The median proportion of staining exceeded those on YL ($Q_{0.5}(I_D) = 0.66$ vs. 0.47). Additionally, while there were often more stained objects as on YL_DEPL, the patterns were (in the median) less fragmented. OL_DEPL B differed from the site OL_DEPL A by a smaller median I_E . In contrast, the distributions of $I_{Q0.95}$, I_F and I_{ME12} on both depletion sites were comparable (Figure 4).

On OL_ACC the staining was larger ($Q_{0.5}(I_D) = 0.36$ vs. 0.14) and there were more large stained objects (Figure 4) compared to the accumulation zone on YL. Moreover, in the median, the patterns were less fragmented. The distributions of I_{ME12} on both accumulation sites were comparable.

Plateau area. The infiltration of the dye tracer on PA was blocked at the interface between the topsoil and the subsoil in approximately 60 cm depth (including the organic layer) (Figure 3). Most of the staining occurred at the interface between the organic horizons and the mineral soil. The distributions of all indices on PA 1 and PA 2 were similar (Figure 4). Except in the profiles closest to the sprinkler, $I_{Q0.95}$ generally did not exceed 0.3 and $I_{Q0.05}$ and $I_{Q0.5}$ were comparable. The largest stained objects were associated with localised quartzite lenses that we found along the interface between the topsoil and the subsoil. Additionally, while preparing the soil profiles we frequently observed roots stained by the dye indicating preferential flow along root macropores, especially in the upper part of the topsoil.

I_F was relatively stable in stained parts of the profiles, while I_D and I_{ME12} fluctuated (Supplementary Figures SF11 and SF12). However, because staining occurred at different depths in different profiles the overall fluctuation was large (Figure 3). Compared to the other experimental sites, the median of the I_E was small because large parts of the profiles were unstained.

In summary, the combination of considerable fragmentation, little variation in metric entropy, moderately large staining and maximal widths indicate that the patterns on YL_DEPL were characterised by a few large and many small stained objects. In contrast, the patterns on YL_ACC contained fewer stained objects than in the depletion zone and were more variable. On OL, the patterns were dominated by a few very large objects that were less fragmented than the respective patterns on the depletion and accumulation zones on YL. Finally, the patterns on PA were localised. While the fragmentation in the stained areas was comparable to YL and OL, the overall fragmentation was small. The patterns were characterised by fewer objects than on the other experimental sites, some of which were large.

4.2.2. Variation with distance

We could distinguish two different groups of experimental sites with regard to relationships between image indices with distance, namely the landslides on the one hand and the plateau area on the other hand (Figure 5). In the first group the normalised mutual information I^* behaved differently for different indices and the curves were spread over the whole range $[0, 1]$. In contrast, in the second group I^* varied in a similar way for all indices and the curves appeared bundled. This confirms the visual impression of similarity between patterns on PA. The profiles at 60 cm, 80 cm and 100 cm on PA 1 are less correlated due to cropping of the

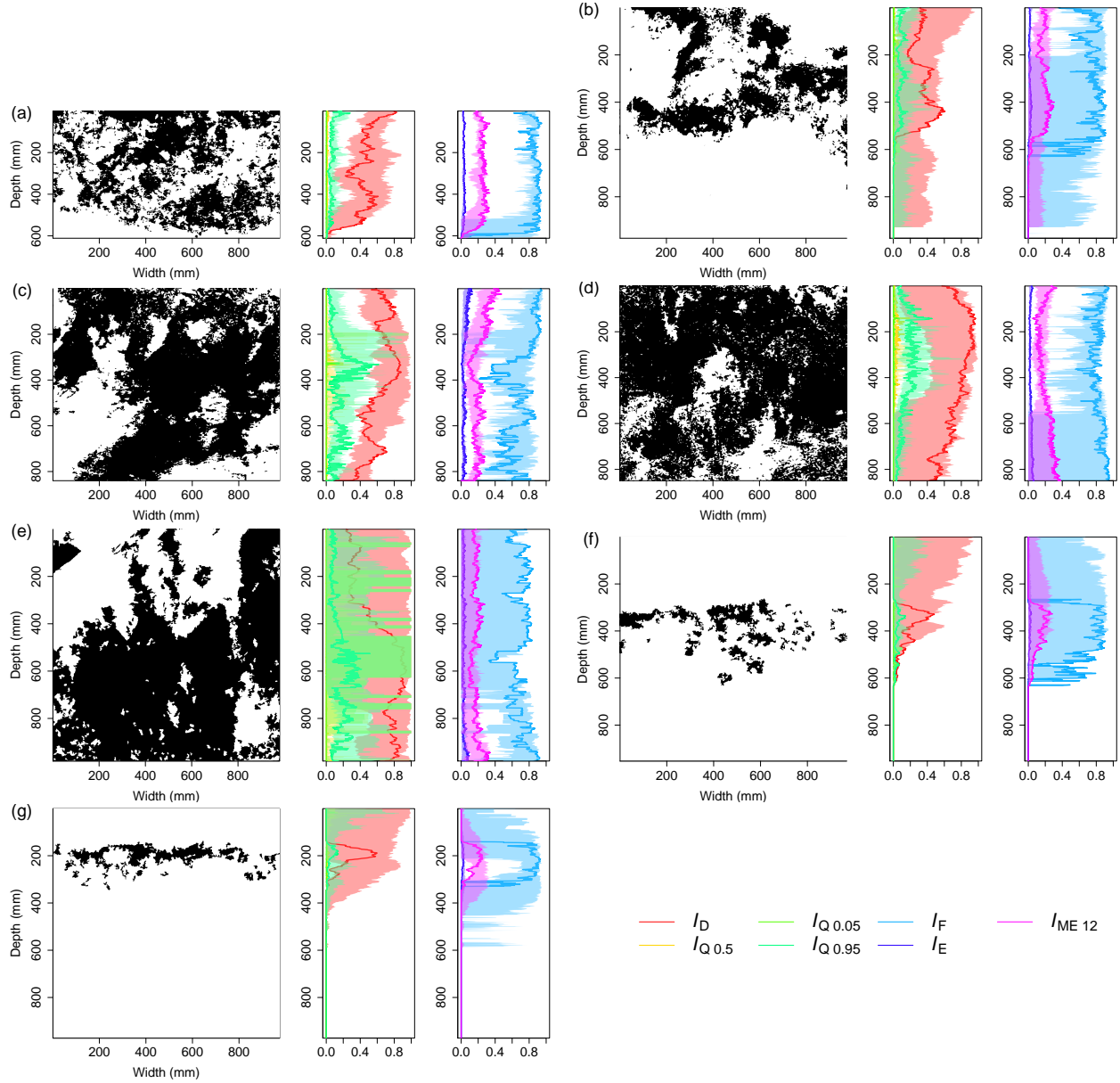


Figure 3: Examples of binary images and their image indices (plain lines): YL_DEPL (a), YL_ACC (b), OL_DEPL A (c), OL_DEPL B (d), OL_ACC B (e), PA 1 (f) and PA 2 (g). The coloured areas show the range of indices on the respective experimental site. All binary images, image indices and their distributions can be found in the online supplementary material.

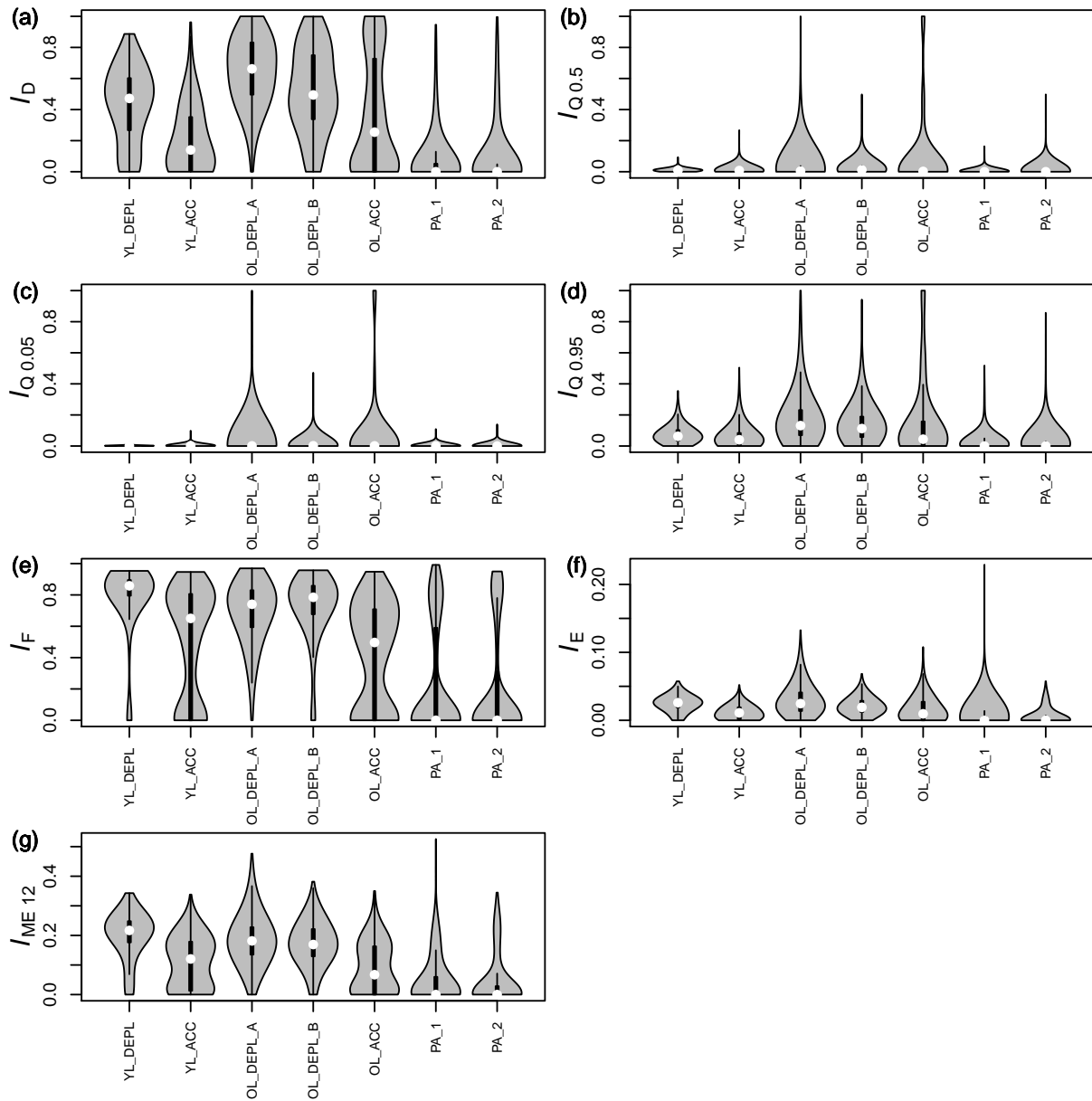


Figure 4: Violin plots of image indices: dye coverage I_D (a), median width of stained objects $I_{Q,0.5}$ (b), minimum width of stained objects $I_{Q,0.05}$ (c), maximum width of stained objects $I_{Q,0.95}$ (d), fragmentation I_F (e), Euler number I_E (f) and metric entropy $I_{ME,12}$ (g). The small black boxes are standard box plots and the white dot indicates the median. The symmetrical areas around the box plots show smoothed density plots.

profile at 80 cm to correct for uneven surface (Supplementary Figure SF11). The site YL_ACC laid somewhat in between: the indices varied more than on PA, however, this variation was comparable between different indices.

Additionally, there was a certain hierarchy of indices. The dye coverage I_D showed the largest I^* on all sites, probably because it varied smoothly with depth. In contrast, the minimum and median widths, $I_{Q0.05}$ and $I_{Q0.5}$, were less dependent or nearly independent like on OL.

When shifting the images, the estimation variability decreased with increasing I^* (i.e. the error bars were smaller) (Figure 6). In general, on landslides the estimates of I^* were comparable between shifted and whole images. Because the patterns on PA were localised and large parts of the profiles unstained, displacing the images with respect to each other strongly affected the calculation of mutual information. Actually, when shifting the images, increasingly more indices of unstained rows were matched with indices of stained rows. This is reflected by a considerable scatter and large error bars in Figure 6. The influence of image shifting on the correlation between images shows that accurate choice of the analysed region of interest is important when patterns are localised.

4.2.3. Comparison between study sites

Similarly to I^* , the PCA separates the study sites into two groups: the landslides and the plateau area. In the former the first two PCs explained most of the variance. In contrast, in the latter the first PC contained more than 97% of the variance (Figure 7).

On YL the original variables (i.e. indices) load in the same sense on the first PC (i.e. all components of the first eigenvector in Figures 8a and 8b are either positive or negative). The second PC contrasts indices related to staining ($I_{Q0.5}$, $I_{Q0.05}$ and $I_{Q0.95}$ and I_D on YL_DEPL) to those reflecting the structure of the patterns (I_F , I_E and I_{ME12}). In other words the first PC separates rows with large indices (i.e. rows with large staining, strong fragmentation and many objects) from those with small indices. On the other hand, the second PC contrasts structure with staining because rows with few large stained objects are separated from rows with many fragmented small objects.

Conversely, on OL_DEPL, staining is contrasted to structure in the first PC and all indices load uniformly on the second PC. On OL_ACC the situation is similar to YL.

On PA all original variables load similarly on the first PC. It separates stained from non-stained regions. In other words the images are partitioned in a part with non-zero vs. a part with zero-valued indices. The variance in the stained areas of the profiles equals less than 3% of the overall variance and is contained in the other PCs.

The confidence intervals obtained by bootstrapping were small indicating a small variation of eigenvalues and eigenvectors in the bootstrapped samples (Figures 7 and 8). Because none of the confidence intervals overlaps zero, we can safely interpret the eigenvector coefficients.

5. Discussion

5.1. Soil physical and hydraulic properties

Soil texture and structure are the main factors that influence the shape of the SWRC (e.g. Nimmo, 1997). Because the textural differences between YL and OL and between the depletion and accumulation zones on the respective landslide are minor, we suppose that

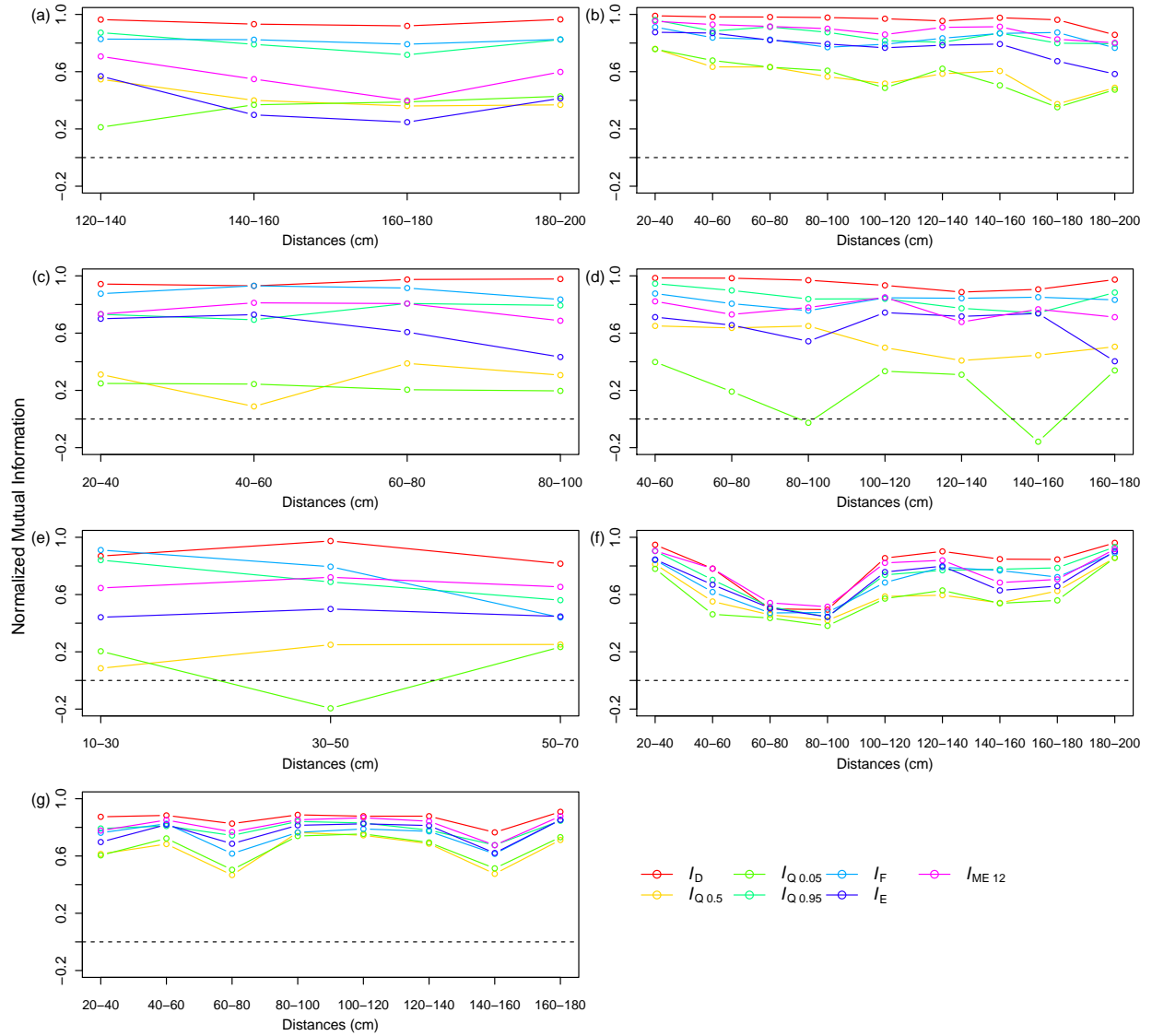


Figure 5: Normalised mutual information: YL_DEPL (a), YL_ACC (b), OL_DEPL A (c), OL_DEPL B (d), OL_ACC B (e), PA 1 (f) and PA 2 (g). Negative values are due to estimation errors.

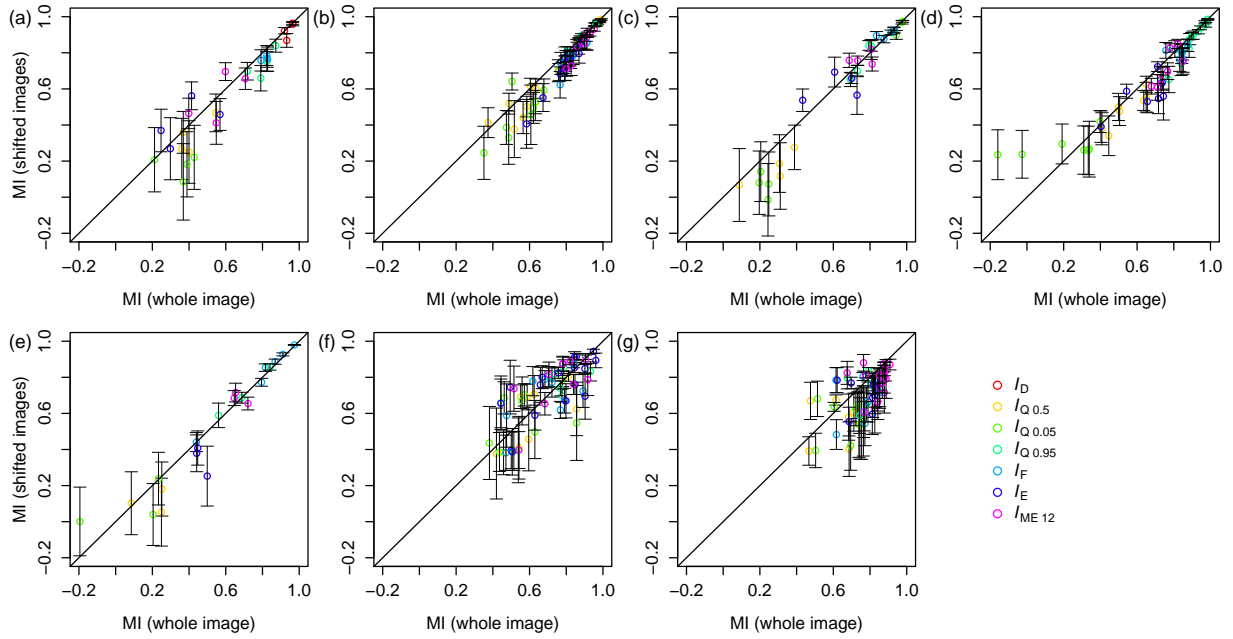


Figure 6: Comparison of mutual information between the whole image and shifted ones: YL_DEPL (a), YL_ACC (b), OL_DEPL A (c), OL_DEPL B (d), OL_ACC B (e), PA 1 (f) and PA 2 (g). Values on the y -axis are means of mutual information on images shifted against each others by $s = 1, 2, \dots, 300$ pixels (approximately 200 mm). The error bars show the 5% and 95% quantiles.

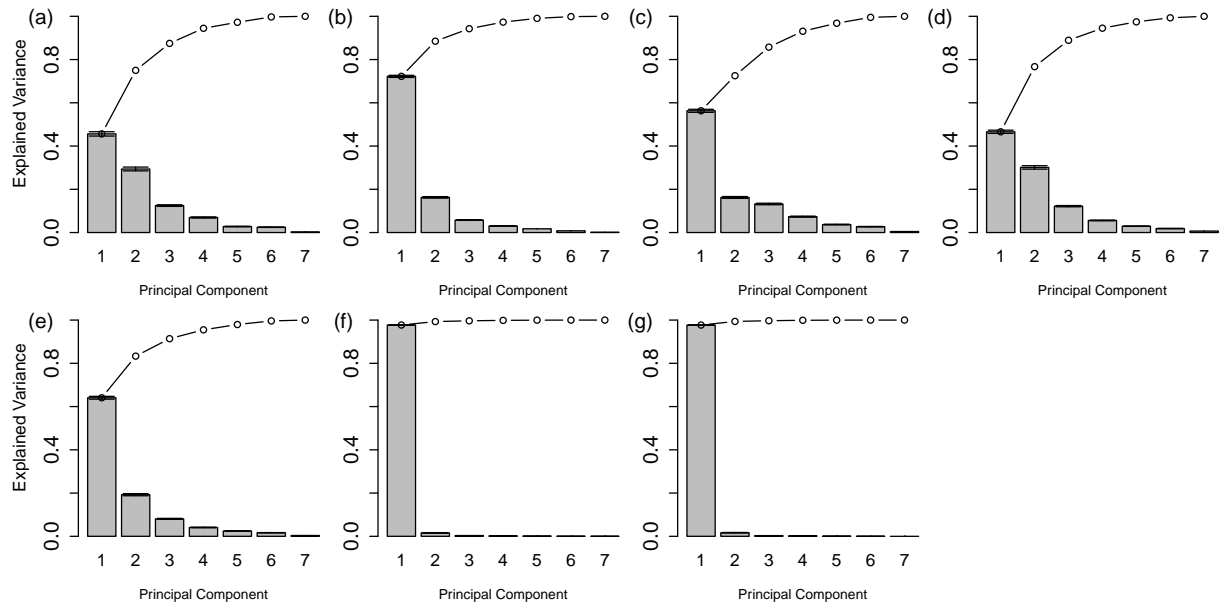


Figure 7: Explained variance from the bootstrapped PCA: YL_DEPL (a), YL_ACC (b), OL_DEPL A (c), OL_DEPL B (d), OL_ACC (e), PA 1 (f) and PA 2 (g). The bars show the explained variance of individual principal components, the dots refer to cumulative explained variance. The error bars indicate the 5% and 95% quantiles.

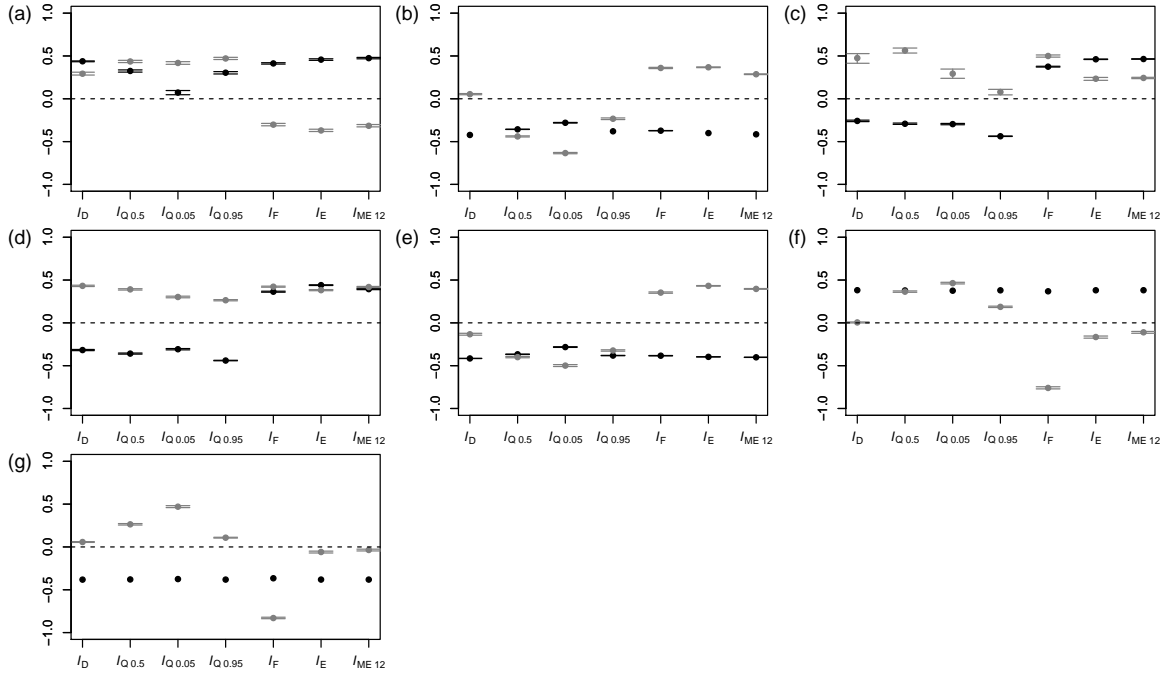


Figure 8: The first (black) and the second (gray) eigenvectors from the bootstrapped PCA: YL_DEPL (a), YL_ACC (b), OL_DEPL A (c), OL_DEPL B (d), OL_ACC (e), PA 1 (f) and PA 2 (g). The error bars show the 5% and 95% quantiles. Error bars for very small errors are not shown.

the distinct shapes of the SWRCs are due to structural differences. Indeed, compaction and deformation during the sliding process as they occur in translational landslides might have destroyed the original soil structure and decreased the porosity. On OL pedogenetic processes acted longer upon regeneration of soil structure than on YL.

An elevated saturated water content on YL_ACC compared to YL_DEPL might be due to a lower bulk density (Table 2). Indeed, Vereecken et al. (1989), for example, found a negative relationship between bulk density and saturated water content. In contrast, the small bulk density on OL_DEPL cannot completely explain the particularly large saturated water content of up to 0.8. Therefore, we assume that organic material has partly been sampled for the SWRCs.

On OL we measured larger K_s values than on YL. There are several factors that can influence K_s such as texture, rock fragment content, porosity or bulk density. The rock fragment content, for example, can increase macroporosity by so-called lacunar pores (i.e. pores at the interface between the rock fragments and the soil matrix) thus increasing K_s (Torri et al., 1994; Sauer and Logsdon, 2002). In other words the positive correlation between the rock fragment content and K_s is probably an indirect one. Indeed, soils of similar rock fragment contents exhibit widely spread K_s values as reported by Sauer and Logsdon (2002), for example. These authors suggested that the adhesion with the surrounding soil matrix might be important: the stronger the rock fragments are held in the soil the weaker is their influence on K_s . In contrast, the relationship between K_s and bulk density is negative (Vereecken et al., 1990).

The sharp boundary between the mineral soil and the parent material on YL-DEPL detected in 25–60 cm depth shows that the sliding process may not be restricted to the organic horizons as assumed by [Wilcke et al. \(2003\)](#), but affects also the mineral soil. This is supported by the K_s measurements that show no decrease with depth and point at a hydrologically homogeneous material. A decrease of K_s with depth has been reported in the literature for other tropical sites (e.g. [Noguchi et al., 2003](#)), as well as for the soils in the RBSF ([Zimmermann and Elsenbeer, 2008](#)).

[Zimmermann and Elsenbeer \(2008\)](#) measured K_s on an old and a young landslides and in a natural forest. In contrast to our study, their results revealed comparable values between the two landslides and between the landslides and the natural forest. Possible explanations for these contradictory findings are the spatial variability of K_s and different ages of the “old” landslides in both studies. While [Zimmermann and Elsenbeer \(2008\)](#) worked on a 7–8 year-old landslide, the old landslide analysed in our study was approximately 50 years old and had a longer regeneration period.

Overall, texture, rock fragment content and root counts were comparable between the landslides (Table 1 and Table 2). However, we observed more macropores on OL than on YL (Supplementary Table ST2) which can partly account for larger K_s on the former. In contrast, differences in rock fragment contents between the landslides and PA might partly explain the lower K_s on the latter. Data on the observed macropores was not available for PA, however, the low root counts can be used as an indicator of a small macroporosity. Additionally, the large bulk densities are in agreement with the low K_s values.

5.2. Relationship between pattern morphology and soil properties

It is difficult to link the indices directly with flow mechanisms because they depict phenomenological aspects of the flow. Indeed, the indices describe the morphology of flow patterns, however, different flow mechanisms can exhibit similar flow patterns. Therefore, it is important to relate additional information on soil properties like rock fragment content or porosity to phenomenological image indices.

Rock fragments can increase dispersion of the water flow and induce so-called funnel flow due to their impervious surfaces. [Bogner et al. \(2008\)](#), for example, sampled soil physical parameters and positions of rock fragments in a skeletal Cambisol ([IUSS Working Group WRB, 2007](#)) in MC 2 (Figure 1) under primary forest. These authors simulated water flow through this soil and showed that rock fragments created preferential flow paths and increased the flow velocity.

Accordingly, we expect larger rock fragment contents to be associated with vaster stained objects. Indeed, I_D and $I_{Q0.95}$, the dye coverage and the maximum width of stained objects, were larger on the landslides than on PA. Moreover, the fragmentation on OL fluctuated stronger because of more variable $I_{Q0.95}$ (c.f. Supplementary Material, section 1.2).

Larger I_D , $I_{Q0.95}$, $I_{Q0.5}$ and $I_{Q0.05}$ on OL compared to YL might be due to more abundant macropores (Supplementary Table ST2) and a stronger macropore–matrix interaction ([Weiler and Flühler, 2004](#)). Indeed, the infiltration from macropores into the soil matrix depends on the hydraulic properties of the latter like saturated and unsaturated hydraulic conductivity and the initial soil moisture (e.g. [Chen and Wagenet, 1992](#); [Weiler and Naef, 2003](#)). Thus, the steeper slope of the SWRCs and the larger K_s values indicate a stronger interaction. In contrast, the flat SWRCs and the small K_s values on YL suggest a weak interaction. Because

the soil matrix remains close to saturation at a broad range of pF values, the infiltration from macropores is limited.

The localised flow patterns on PA are probably related to low rock fragment content, few roots and low K_s . This local character is well reflected by the PCA. Actually, most of the variance in the image indices on these experimental sites is contained in the first principal component that separates stained from non-stained areas. The second principal component that distinguishes details in the stained patterns explains only little variance. In contrast, the first two PCs on the landslides are related to staining and structure of the patterns.

The mutual information I^* between phenomenological image indices captures the relationship between adjacent soil profiles and thus describes the third dimension in the flow patterns. On PA, for example, I^* varied similarly with distance to the sprinkler for different indices. This supports the visually perceived similarity between patterns of subsequent profiles. Actually, because staining occurred mainly at the interface between the organic horizons and the mineral soil, we assume that part of the dye travelled as interflow. As this interface remains in approximately the same depth between adjacent profiles the stained patterns are comparable. A similar argument applies to YL_ACC where all indices of subsequent profiles were largely related. There, the similarity between the patterns might be due to the fissure network that connects the adjacent profiles.

5.3. Implications for hydrology of studied landslides

On YL fissures that were possibly caused by a slow mass movement might be an important factor controlling the hydrological behaviour of the landslide. The importance of preferential flow (including flow through fissures) on landslides and hillslopes has been reported by several authors (e.g. McDonnell, 1990; Fannin et al., 2000; Uchida et al., 2001). In a recent paper, Krzeminska et al. (2012) analysed the spatial and temporal variation of the fissure network via modelling. Their results suggest that the permeability and connectivity of fissures were important factors that control the distribution of water in a landslide. The temporal changes of fissures like opening/closing due to mass movement or soil moisture and the degree of connectivity make the network highly dynamic.

On YL_ACC, for example, we found several fissures reaching deep into the soil (Supplementary Figures SF13 and SF14). Smaller fissures were visible on YL_DEPL. Thus, during rainstorm events, water might infiltrate along the fissure network and a subsurface flow might occur along the interface to the weathered bedrock. Similar results were described by McDonnell (1990) who studied a debris flow in New Zealand. He reported a fast infiltration of water via fissures and its distribution through a pipe system at the soil–bedrock interface.

Although we lack detailed information on the topography of the soil–bedrock interface, the variable soil thickness on YL_DEPL indicates possible depressions and ridges. In their “fill and spill” hypotheses, Tromp-van Meerveld and McDonnell (2006) emphasised the influence of depressions and their connectivity on hillslope hydrology. They argued that first the depressions filled before water was spilled over and the subsurface saturated areas became connected increasing the subsurface stormflow.

Another interface, namely the one between the organic layer and the mineral soil, appears to play an important role on infiltration and water flow on OL and PA. On the former, part of the tracer concentrated in a depression that could thus be an area of preferential infiltration. Furthermore, because on both studied sites part of the tracer flowed along the organic–mineral

interface, its microtopography might be important for initiation of subsurface flow via a “fill and spill” mechanism.

6. Summary and conclusions

We have studied the morphology of flow patterns on a young and an old landslides and a landslide-unaffected site by combining information from morphological image indices with soil hydrological properties and field observations. Our data have shown, that a larger rock fragment content on the landslides is associated with larger stained objects characterised by morphological indices I_D and $I_{Q0.95}$. Despite a comparable K_s on the young landslide and the landslide-unaffected site, the dye infiltrated deeper into the soil on the former. This is probably related to a fissure network on the landslide.

Additionally, we quantified the relationship between the pattern morphology in adjacent soil profiles via the mutual information between image indices. This relationship is seldom taken into account in tracer studies and describes the third dimension in the flow patterns. On the landslide-unaffected site, the topography of the interface between the organic horizons and the mineral soil probably leads to preferential infiltration in depressions and an interflow. In the depletion zone on the young landslide a network of fissures might lead to preferential infiltration and a subsurface flow via a “fill and spill” mechanism. On these sites, the mutual information indicates a strong relationship between the morphology of indices in adjacent soil profiles. In contrast, on the old landslide, the mutual information varies to a greater extend between soil profiles. At this study, the organic–mineral soil interface affects the flow, but also a large stone content, a greater macroporosity and a stronger macropore–soil matrix interaction.

We have shown that a collection of morphological image indices have the potential to detect more details in flow patterns than the dye coverage alone. Features like fragmentation or small-scale correlation (metric entropy) might be relevant when comparing different sites. The multivariate data analysis by PCA yields further insight by identifying similarities and differences between study sites.

K_s , SWRCs and tracer experiments characterise different hydrological aspects of the studied sites. While dye tracer studies with a large irrigation rate emphasise the macrostructure of the soil and reveal large features like fissure networks, K_s and SWRC help to understand the macropore–soil matrix interaction, for example. Finally, field observations, profile description and soil properties complement the information provided by the morphological image indices.

Acknowledgements

We are grateful to Iris Schmiedinger, Andreas Kolb, Ingrid Hausinger, Lisa Höhn, Stefanie Schier, Tobias Biermann, Lutz Breuer and Daniela Vasquez for their help in the laboratory and during the field experiments. We thank the reviewers for helpful comments on the manuscript. This study was funded by the German Research Foundation Grant No. DFG FOR 402/1-1 Hu 636/9-3 and DFG FOR 816-HU 636/14-1.

Appendix A. Supplementary material

Supplementary data associated with this article can be found, in the online version, at <http://dx.doi.org/10.1016/j.jhydrol.2014.01.063>.

References

- Adams, P.W., Sidle, R.C., 1987. Soil conditions in three recent landslides in Southeast Alaska. *Forest Ecology and Management* 18, 93–102.
- AG Boden, 2005. *Bodenkundliche Kartieranleitung*. Bundesanstalt für Geowissenschaften und Rohstoffe und Geologische Landesämter der Bundesrepublik Deutschland. 5th edition. In German.
- Amoozegar, A., 1989a. A compact constant-head permeameter for measuring saturated hydraulic conductivity of the vadose zone. *Soil Science Society of America Journal* 53, 1356–1361.
- Amoozegar, A., 1989b. Comparison of the Glover solution with the simultaneous-equations approach for measuring hydraulic conductivity. *Soil Science Society of America Journal* 53, 1362–1367.
- Balslev, H., Øllgaard, B., 2002. Mapa de vegetación del sur de Ecuador, in: Aguirre, Z., Madsen, J., Cotton, E., Balslev, H. (Eds.), *Botánica austroecuatoriana: estudios sobre los recursos vegetales en las provincias de El Oro, Loja y Zamora-Chinchipec*. Abya Yala, Quito (Ecuador), pp. 51–64.
- Beck, E., Bendix, J., Kottke, I., Makeschin, F., Mosandl, R. (Eds.), 2008. *Gradients in a Tropical Mountain Ecosystem of Ecuador*. Springer. ISBN 978-3-540-73525-0.
- Bendix, J., Beck, E., Bräuning, A., Makeschin, F., Mosandl, R., Scheu, S., Wilcke, W. (Eds.), 2013. *Ecosystem Services, Biodiversity and Environmental Change in a Tropical Mountain Ecosystem of South Ecuador*. Springer. ISBN: 978-3-642-38136-2.
- Bogner, C., Engelhardt, S., Zeilinger, J., Huwe, B., 2008. Visualization and analysis of flow patterns and water flow simulations in disturbed and undisturbed tropical soils, in: Beck, E., Bendix, J., Kottke, I., Makeschin, F., Mosandl, R. (Eds.), *Gradients in a Tropical Mountain Ecosystem of Ecuador*. Springer, Berlin Heidelberg, volume 198 of *Ecological Studies*, pp. 387–396.
- Bogner, C., Trancón y Widemann, B., Lange, H., 2013. Characterising flow patterns in soils by feature extraction and multiple consensus clustering. *Ecological Informatics* 15, 44–52.
- Borg, I., Groenen, P., 2005. *Modern multidimensional scaling: Theory and applications*. Springer. ISBN 978-0-387-25150-9.
- Bussmann, R., Wilcke, W., Richter, M., 2008. Landslides as important disturbance regimes – causes and regeneration, in: Beck, E., Bendix, J., Kottke, I., Makeschin, F., Mosandl, R. (Eds.), *Gradients in a tropical mountain ecosystem of Ecuador*. Springer, pp. 319–330.
- Cendrero, A., Dramis, F., 1996. The contribution of landslides to landscape evolution in Europe. *Geomorphology* 15, 191–211.
- Chen, C., Wagenet, R., 1992. Simulation of water and chemicals in macropore soils Part 1. Representation of the equivalent macropore influence and its effect on soilwater flow. *Journal of Hydrology* 130, 105–126.
- Crozier, M.J., 1986. *Landslides: Causes, consequences and environment*. Croom Helm.
- Cruden, D., 1991. A simple definition of a landslide. *Bulletin of Engineering Geology and the Environment* 43, 27–29.

- Cruden, D.M., Varnes, D.J., 1996. Landslide types and processes, in: *Landslides: investigation and mitigation*. Transportation Research Board Special Report. volume 247, pp. 36–75.
- Efron, B., Tibshirani, R., 1986. Bootstrap methods for standard errors, confidence intervals, and other measures of statistical accuracy. *Statistical Science* 1, 54–75.
- Fannin, R., Jaakkola, J., Wilkinson, J., Hetherington, E., 2000. Hydrologic response of soils to precipitation at carnation creek, british columbia, canada. *Water Resources Research* 36, 1481–1494.
- FAO, 2006. Guidelines for soil description. Technical Report. Food and Agriculture Organization of the United Nations. Rome.
- Fleischbein, K., Wilcke, W., Goller, R., Boy, J., Valarezo, C., Zech, W., Knoblich, K., 2005. Rainfall interception in a lower montane forest in Ecuador: effects of canopy properties. *Hydrological Processes* 19, 1355–1371.
- Flury, M., Flühler, H., Jury, W.A., Leuenberger, J., 1994. Susceptibility of soils to preferential flow of water: a field study. *Water Resources Research* 30, 1945–1954.
- Garwood, N.C., Janos, D.P., Brokaw, N., 1979. Earthquake-caused landslides: A major disturbance to tropical forests. *Science* 205, 997–999.
- van Genuchten, M.T., 1980. A closed form equation for predicting the hydraulic conductivity of unsaturated soils. *Soil Science Society of America Journal* 44, 892–898.
- Guariguata, M.R., 1990. Landslide disturbance and forest regeneration in the Upper Luquillo Mountains of Puerto Rico. *Journal of Ecology* 78, 814–832.
- Guzzetti, F., Peruccacci, S., Rossi, M., Stark, C., 2008. The rainfall intensity–duration control of shallow landslides and debris flows: an update. *Landslides* 5, 3–17.
- Hintze, J.L., Nelson, R.D., 1998. Violin plots: A box plot-density trace synergism. *The American Statistician* 52, 181–184.
- Homeier, J., Dalitz, H., Breckle, S., 2002. Waldstruktur und Baumartendiversität im montanen Regenwald der Estación Científica San Francisco in Südecuador. *Berichte der Reinhold-Tüxen-Gesellschaft* 14, 109–118. In German.
- Hungerbühler, D., 1997. Neogene basins in the Andes of southern Ecuador: evolution, deformation and regional tectonic implications. Ph.D. thesis. ETH Zürich. Zürich, Switzerland.
- IUSS Working Group WRB, 2007. World reference base for soil resources 2006, first update 2007. World Soil Resources Reports No. 103. FAO, Rome. http://www.fao.org/fileadmin/templates/nr/images/resources/pdf_documents/wrb2007_red.pdf. [Accessed in January 2014].
- Jackson, D., 1993. Stopping rules in principal components analysis: a comparison of heuristical and statistical approaches. *Ecology* 74, 2204–2214.
- Jarvis, N.J., 2007. A review of non-equilibrium water flow and solute transport in soil macropores: principles, controlling factors and consequences for water quality. *European Journal of Soil Science* 58, 523–546.
- Joe, H., 1989. Relative entropy measures of multivariate dependence. *Journal of the American Statistical Association* 84, 157–164.
- Kessler, M., 1999. Plant species richness and endemism during natural landslide succession in a perhumid montane forest in the Bolivian Andes. *Ecotropica* 5, 123–136.

- Kraskov, A., Stögbauer, H., Grassberger, P., 2004. Estimating mutual information. *Physical Review E* 69, 066138.
- Krzeminska, D.M., Bogaard, T.A., van Asch, T.W.J., van Beek, L.P.H., 2012. A conceptual model of the hydrological influence of fissures on landslide activity. *Hydrology and Earth System Sciences* 16, 1561–1576.
- Köhn, M., 1928. Bemerkungen zur mechanischen Bodenanalyse. III. Ein neuer Pipettapparat. *Zeitschrift für Pflanzenernährung, Düngung, Bodenkunde* 11, 50–54. In German.
- Liess, M., Glaser, B., Huwe, B., 2009. Digital soil mapping in Southern Ecuador. *Erdkunde* 63, 309–319.
- Lundgren, L., 1978. Studies of soil and vegetation development on fresh landslide scars in the Mgeta Valley, Western Uluguru Mountains, Tanzania. *Geografiska Annaler. Series A, Physical Geography* 60, 91–127.
- Markwardt, S., 2005. Validity of two pedotransfer functions in two microcatchments of a tropical mountain rainforest in Southern Ecuador. Unpublished diploma thesis. University of Bayreuth. Bayreuth, Germany.
- McDonnell, J., 1990. The influence of macropores on debris flow initiation. *Quarterly Journal of Engineering Geology and Hydrogeology* 23, 325–331.
- Mehlman, D., Shepherd, U., Kelt, D., 1995. Bootstrapping principal components analysis: a comment. *Ecology* 76, 640–643.
- MVTec Software GmbH, 2007. Solution Guide I. Basics.
- Nimmo, J.R., 1997. Modeling structural influences on soil water retention. *Soil Science Society of America Journal* 61, 712–719.
- Noguchi, S., Kasran, B., Yusop, Z., Tsuboyama, Y., Tani, M., 2003. Depth and physical properties of soil in a forest and a rubber plantation in peninsular malaysia. *Journal of Tropical Forest Science* 15, 513–530.
- Noguchi, S., Tsuboyama, Y., Sidle, R., Hosoda, I., 1999. Morphological characteristics of macropores and the distribution of preferential flow pathways in a forested slope segment. *Soil Science Society of America Journal* 63, 1413–1423.
- Numata, J., Ebenhöf, O., Knapp, E., 2008. Measuring correlations in metabolomic networks with mutual information. *Genome Informatics* 20, 112–122.
- Oyama, M., Takehara, H., 1999. Revised standard soil color charts. Eijkelkamp Agrisearch Equipment, Soil colour book 08.11, Netherlands.
- Paulsch, A., 2002. Development and application of a classification system for undisturbed and disturbed tropical montane forests based on vegetation structure. Ph.D. thesis. University of Bayreuth. Bayreuth, Germany.
- Pyle, D., 1999. Data preparation for data mining. Morgan Kaufmann Publishers, Inc.
- Rollenbeck, R., Bendix, J., Fabian, P., Boy, J., Wilcke, W., Dalitz, H., Oesker, M., Emck, P., 2007. Comparison of different techniques for the measurement of precipitation in tropical montane rain forest regions. *Journal of Atmospheric and Oceanic Technology* 24, 156–168.
- Sales, G., Romualdi, C., 2012. parmigene: Parallel Mutual Information estimation for Gene Network reconstruction. R package version 1.0.2.
- Sauer, T.J., Logsdon, S.D., 2002. Hydraulic and physical properties of stony soils in a small watershed. *Soil Science Society of America Journal* 66, 1947–1956.

- Torri, D., Poesen, J., Monaci, F., Busoni, E., 1994. Rock fragment content and fine soil bulk density. *Catena* 23, 65–71.
- Tromp-van Meerveld, H., McDonnell, J., 2006. Threshold relations in subsurface stormflow: 2. The fill and spill hypothesis. *Water Resources Research* 42, W02411.
- Uchida, T., Kosugi, K., Mizuyama, T., 2001. Effects of pipeflow on hydrological process and its relation to landslide: a review of pipeflow studies in forested headwater catchments. *Hydrological Processes* 15, 2151–2174.
- Varnes, D.J. and the International Association Of Engineering Geology Commission on Landslides and Other Mass Movements on Slopes, 1984. *Landslide hazard zonation: a review of principles and practice*. Technical Report. UNESCO.
- Vereecken, H., Maes, J., Feyen, J., 1990. Estimating unsaturated hydraulic conductivity from easily measured soil properties. *Soil Science* 149, 1–12.
- Vereecken, H., Maes, J., Feyen, J., Darius, P., 1989. Estimating the soil moisture retention characteristic from texture, bulk density, and carbon content. *Soil Science* 148, 389–403.
- Weiler, M., Flühler, H., 2004. Inferring flow types from dye patterns in macroporous soils. *Geoderma* 120, 137–153.
- Weiler, M., Naef, F., 2003. An experimental tracer study of the role of macropores in infiltration in grassland soils. *Hydrological Processes* 17, 477–493.
- Werner, F.A., Homeier, J., Gradstein, S.R., 2005. Diversity of vascular epiphytes on isolated remnant trees in the montane forest belt of southern Ecuador. *Ecotropica* 11, 21–40.
- Trancón y Widemann, B., Bogner, C., 2012. Image analysis for soil dye tracer infiltration studies, in: *Proceedings of the 3rd International Conference on Image Processing Theory, Tools and Applications*, pp. 409–414. <http://dx.doi.org/10.1109/IPTA.2012.6469517>.
- Wilcke, W., Valladares, H., Stoyan, R., Yasin, S., Valarezo, C., Zech, W., 2003. Soil properties on a chronosequence of landslides in montane rain forest, Ecuador. *Catena* 53, 79–95.
- Wilcke, W., Yasin, S., Valarezo, C., Zech, W., 2001. Change in water quality during the passage through a tropical montane rain forest in Ecuador. *Biogeochemistry* 55, 45–72–72.
- Wolf, F., 1999. *Berechnung von Information und Komplexität in Zeitreihen – Analyse des Wasserhaushaltes von bewaldeten Einzugsgebieten*. Ph.D. thesis. University of Bayreuth. In German.
- Yasin, S., 2001. *Water and nutrient dynamics in microcatchments under montane forest in the South Ecuadorian Andes*. Bayreuther Bodenkundliche Berichte, 73, University of Bayreuth.
- Zimmermann, B., Elsenbeer, H., 2008. Spatial and temporal variability of soil saturated hydraulic conductivity in gradients of disturbance. *Journal of Hydrology* 361, 78–95.